Natural Resources Canada | Ressources naturelles Canada

GEOMATICS CANADA
OPEN FILE 70

A report on water quality monitoring in Quesnel Lake, British Columbia, subsequent to the Mount Polley tailings dam spill, using optical satellite imagery

M. Hodul, H.P. White, and A. Knudby

2022

Canada

GEOMATICS CANADA
OPEN FILE 70

A report on water quality monitoring in Quesnel Lake, British Columbia, subsequent to the Mount Polley tailings dam spill, using optical satellite imagery

M. Hodul[1, 2], H.P. White[1], and A. Knudby[2]

[1]Canada Centre for Mapping and Earth Observations, 560 Rochester Street, Ottawa, Ontario
[2]Department of Geography, Environment and Geomatics, University of Ottawa, 60 University, Ottawa, Ontario

2022

Permanent link: https://doi.org/10.4095/330556

This publication is available for free download through GEOSCAN (https://geoscan.nrcan.gc.ca/).

Recommended citation
Hodul, M., White, H.P., and Knudby, A., 2022. A report on water quality monitoring in Quesnel Lake, British Columbia, subsequent to the Mount Polley tailings dam spill, using optical satellite imagery; Geomatics Canada, Open File 70, 1. zip file. https://doi.org/10.4095/330556

Publications in this series have not been edited; they are released as submitted by the author.

1. Introduction

In the early morning on the 4th of August 2014, a tailings dam near Quesnel, BC, burst, spilling approximately 25 million m^3 of runoff containing heavy metal elements into nearby Quesnel Lake (Byrne et al. 2018). The runoff slurry, which included lead, arsenic, selenium, and vanadium spilled through Hazeltine Creek, scouring its banks and picking up till and forest cover on the way, and ultimately ended up in Quesnel Lake, whose water level rose by 1.5 m as a result. While the introduction of heavy metals into Quesnel Lake was of environmental concern, the additional till and forest cover scoured from the banks of Hazeltine Creek added to the lake has also been of concern to salmon spawning grounds.

Immediate repercussions of the spill involved the damage of sensitive environments along the banks and on the lakebed, the closing of the seasonal salmon fishery in the lake, and a change in the microbial composition of the lake bed (Hatam et al. 2019). In addition, there appears to be a seasonal resuspension of the tailings sediments due to thermal cycling of the water and surface winds (Hamilton et al. 2020).

While the water quality of Quesnel Lake continues to be monitored for the tailings sediments, primarily by members at the Quesnel River Research Centre, the sample-and-test methods of water quality testing used, while highly accurate, are expensive to undertake, and not spatially exhaustive. The use of remote sensing techniques, though not as accurate as lab testing, allows for the relatively fast creation of expansive water quality maps using sensors mounted on boats, planes, and satellites (Ritchie et al. 2003).

The most common method for the remote sensing of surface water quality is through the use of a physics-based semi analytical model which simulates light passing through a water column with a given set of Inherent Optical Properties (IOPs), developed by Lee et al. (1998) and commonly referred to as a Radiative Transfer Model (RTM). The RTM forward-models a wide range of water-leaving spectral signatures based on IOPs determined by a mix of water constituents, including natural materials and pollutants. Remote sensing imagery is then used to invert the model by finding the modelled water spectrum which most closely resembles that seen in the imagery (Brando et al 2009).

This project set out to develop an RTM water quality model to monitor the water quality in Quesnel Lake, allowing for the entire surface of the lake to be mapped at once, in an effort to easily determine the timing and extent of resuspension events, as well as potentially investigate greening events reported by locals. The project intended to use a combination of multispectral imagery (Landsat-8 and Sentinel-2), as well as hyperspectral imagery (DESIS – The DLR Earth Sensing Imaging Spectrometer), combined with field calibration/validation of the resulting models.

The project began in the autumn before the COVID pandemic, with plans to undertake a comprehensive fieldwork campaign to gather model calibration data in the summer of 2020. Since a province-wide travel shutdown and social distancing procedures made it difficult to carry out water quality surveying in a small boat, an insufficient amount of fieldwork was conducted to suit the needs of the project. Thus, the project has been put on hold, and the primary researcher has moved to a

different project. This document stands as a report on all of the work conducted up to April 2021, intended largely as an instructional document for researchers who may wish to continue the work once fieldwork may freely and safely resume.

This research was undertaken at the University of Ottawa, with supporting funding provided by the Earth Observations for Cumulative Effects (EO4CE) Program Work Package 10b: Site Monitoring and Remediation, Canada Centre for Remote Sensing, through the Natural Resources Canada Research Affiliate Program (RAP).

2. Technical Background

Certain water quality parameters may be extracted from the spectral signature of water-leaving reflectance (Rrs) at the top of the water column, which can be measured by remote sensing systems (Dekker et al. 2011). Rrs is defined as the ratio of irradiance to water-leaving radiance (so not including surface reflectance off of the water), per unit of solid angle (steradian). The Inherent Optical Properties (IOPs) of the water column, which inform Rrs, are directly influenced by optically active constituents in the water (Ogashawara et al. 2017), and the amount of these constituents present in the water is one working definition of water quality. A range of available physics models may be used to forward-model the expected Rrs given a set of optically active constituents, and the model can then be inverted, comparing the modelled Rrs to imagery-observed Rrs to determine water quality.

2.1 Water Quality and Inherent Optical Properties

Water quality, for the purpose of remote sensing applications, may be described by three optically active water constituents (Ogashawara et al. 2017):

- **Chlorophyll-a -** chl-a, which acts as the optically active surrogate for the microscopic phytoplankton, is a green pigment present in all photosynthesizing organisms (Matthews 2017). Though we can't observe individual phytoplankton, the cumulative effect of the chl-a pigment is easily observable in remote sensing imagery. Phytoplankton is an important water quality metric to monitor, as the presence of certain kinds of these organisms may increase the levels of harmful toxins in the water. Chl-a absorbs strongly around 440 nm and 670 nm, resulting in the green colour associated with vegetation, but depending on the particulars of the phytoplankton, there may be accompanying red or brown pigments as well.
- **Coloured Dissolved Organic Matter -** CDOM acts as the optically active proxy for the total level of Dissolved Organic Carbon (DOC). The presence of DOC in water obscures light entering the water and reduces the efficacy of chlorination as a water treatment technique for drinking water (Kutser et al. 2017) and is thus of interest to water quality monitoring. CDOM tends to absorb strongly in the blue spectrum and very little in red, leading to its yellow/brown colour.

- **Total Suspended Solids -** TSS is an important water quality constituent, as it influences sedimentation processes, obscures river-bottom vegetation from the sunlight they need, may provide food for organisms in the water, and may carry harmful toxins (Giardino et al. 2017). TSS may be composed of a number of materials, including minerals, organic matter and detritus, and bacteria, among others, though notably do not include large floating objects such as logs, and do not include settled matter such as large boulders. Spectral properties of TSS vary widely due to the nature of the component particles making it a challenge aspect in remote sensing application development.

Pure water also has an effect on the IOPs of a water column, though this is well defined empirically.

These three constituents, along with the fundamental properties of pure water and, in the case of optically shallow water (water in which the bottom plays a role in light propagation back to the surface), depth and bottom reflectance, define a water column's IOPs. These IOPs contribute to Rrs, which is the property measured by remote sensing (Brando et al. 2009) and field spectroscopy (Lee et al. 2013).

2.2 Physic-Based Water Quality Modelling

It is possible to simulate what R_{rs} will be for a water column given a particular set of environmental variables (chl-a, CDOM, TSS, depth, and bottom reflectance) using physics-based models (Lee et al. 1998). To invert the model on remote sensing imagery, we run the simulation hundreds (perhaps thousands) of times with a range of environmental variables which can be reasonably expected to occur in our area of interest, constructing a Look-Up Table (LUT). Finding the R_{rs} value in the LUT which most closely resembles that seen in atmospherically corrected imagery of our area of interest then gives us the corresponding environmental variables which created that particular R_{rs} (see Figure 1 for process flowchart). This is repeated for each water pixel in a scene or area of interest.

The most commonly used physics-based model for this is the one proposed by Lee et al. (1998), or some subsequent variant thereof, such as the Semi-Analytical Model for Bathymetry, Unmixing, and Concentration Assessment (SAMBUCA) (Brando et al. 2009). Most of these models are quite similar, varying just in the particular empirical tuning factors used; the Lee model is demonstrated below. The model is run individually for each wavelength desired, typically run at 1 nm increments to create an effectively continuous spectrum, and then convolved to match the desired spectral response curves of the imagery.

R_{rs}, the reflectance just above the water surface and the value seen by remote sensing imagery, is calculated from r_{rs}, the reflectance just below the water surface, as

$$R_{rs} = \frac{0.518 r_{rs}}{1.0 - 1.562 r_{rs}}$$

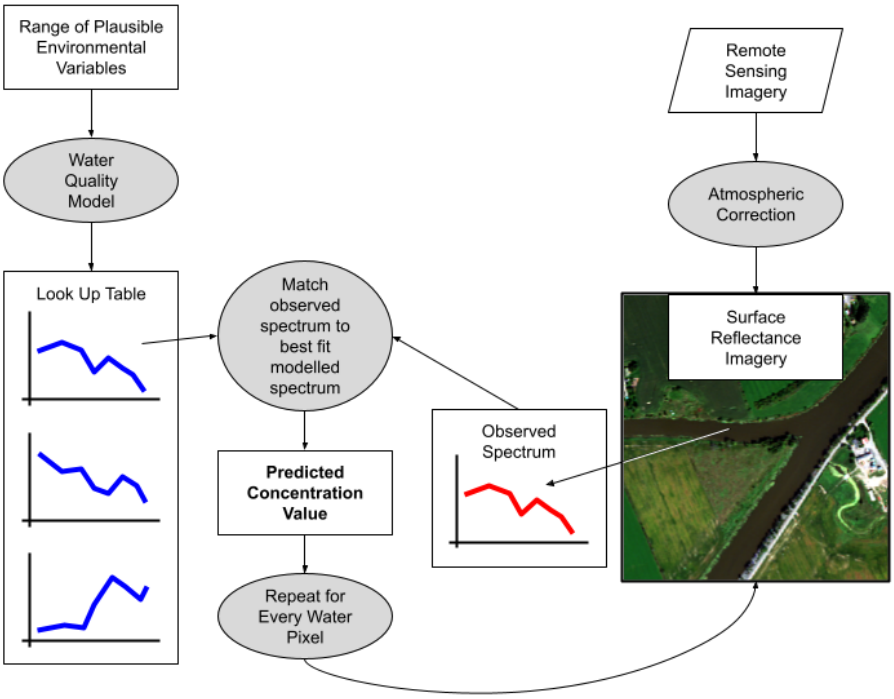

Figure 1: Flowchart illustrating the modelling and inversion workflows of water quality modelling.

where r_{rs} is given by

$$r_{rs} = (0.070{+}0.155u^{0.752})u{\cdot}\left(1 - 1.03\exp\left\{-\left[\frac{1}{cos(\theta_w)} + 1.2(1+2.0u)^{0.5}\alpha H\right]\right\}\right)$$
$$+0.31\rho\exp\left\{-\left[\frac{1}{cos(\theta_w)} + 1.2(1+2.0u)^{0.5}\alpha H\right]\right\}$$

where θ_w is the subsurface solar zenith angle, and ρ and H are bottom reflectance and depth. u and α are defined as

$$u \equiv \frac{b_t}{b_t + a_t} \quad \alpha \equiv a_t + b_t$$

a_t and b_t are the total backscattering and absorption within the water column. Total absorption a_t is given by the sum of absorption factors from pure water a_w, phytoplankton a_{phy}, and CDOM a_{cdom}. The pure water absorption spectrum a_w is a well understood, laboratory measured spectrum (Figure 2).

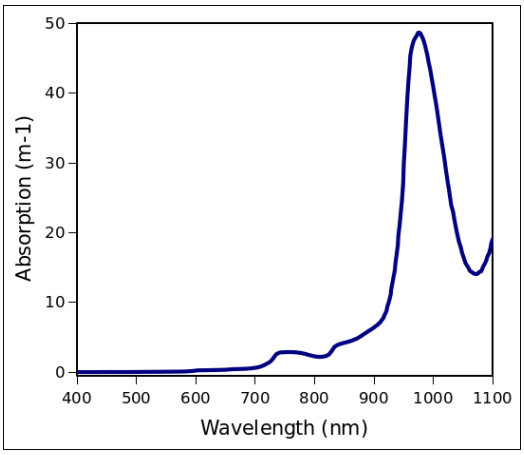

Figure 2: Laboratory-measured absorption spectrum of pure water.

a_{phy} and a_{cdom} vary as a function of the concentrations of chl-a and CDOM respectively (C_{chl} and C_{cdom}), described by

$$a_{phy}(\lambda) = C_{chl}(a^*_{phy}(\lambda) + a'_{phy})$$

where a^*_{phy} is an absorption spectrum coefficient (Figure 3):

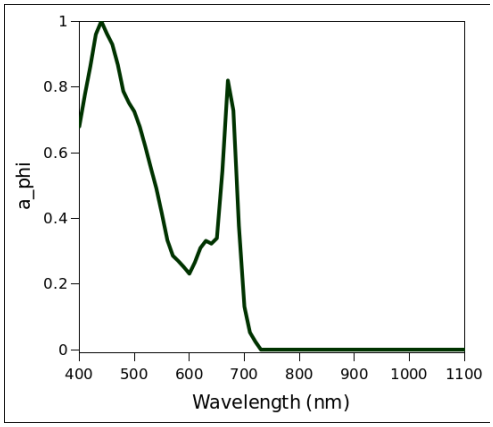

Figure 3: Phytoplankton absorption coefficient.

and $a`_{phy}$ is an empirically tuned scalar operator; and

$$a_{cdom}(\lambda) = D_{cdom} \cdot a^*_{cdom}(\lambda_{0cdom}) e^{-S_{cdom}(\lambda - \lambda_{0cdom})}$$

where $a^*_{cdom(\lambda_{0cdom})}$ is the absorption coefficient at a reference wavelength, S_{cdom} is the slope of the CDOM absorption curve (or spectral decay constant), and λ_{0cdom} is the reference wavelength.

Total backscatter b_t is given by the sum of backscattering factors from phytoplankton b_{phy} and TSS b_{tss}, which vary as a function of the concentrations of chl-a and TSS (C_{chl} and C_{tss}) described by,

$$b_{bphy}(\lambda) = C_{phy} \cdot b^*_{bphy}(\lambda_{0bphy})(\lambda_{0bphy}/\lambda)^{Y_{phy}}$$

Where $b^*_{bphy(\lambda_{0bphy})}$ is the scatter coefficient at a reference wavelength, Y_{phy} is an empirical constant, and λ_{0bphy} is the reference wavelength; and

$$b_{bnap}(\lambda) = C_{nap} \cdot b^*_{bnap}(\lambda_{0bnap})(\lambda_{0bnap}/\lambda)^{Y_{nap}}$$

With parameters similar to those above.

Important to note is that all equations for the individual backscattering and absorption factors, with the exception of the simple water absorption spectrum, include empirically-tuned physical parameters, the exact values of which are a subject of ongoing research, likely vary depending on specifics of the water body under investigation, and may require field measurement to fine-tune to a precise level.

Using these equations, the LUT is developed for a range of expected environmental parameters, and the model may be inverted on the imagery. Inversion is typically done by measuring *optical closure* (Brando et al. 2009), which calculates how similar the observed R_{rs} is to each modelled R_{rs} in the LUT, and may be as simple as calculating the Root Mean Square Error (RMSE) between the modelled and observed values for each band. A more complicated optical closure calculation, like the one in SAMBUCA, may also involve a measure of the shape of each spectrum independent of its magnitude. In these equations, optical closure Δ is given by

$$\Delta \equiv \alpha \cdot LSQ$$

$$\alpha = cos^{-1}\frac{\sum w(\lambda) \cdot r_{lut} \cdot r_{pxl}}{\left[\sum (w(\lambda) \cdot r_{lut})^2\right]^{1/2} \cdot \left[\sum (w(\lambda) \cdot r_{pxl})^2\right]^{1/2}}$$

$$LSQ = \frac{\left[\sum w(\lambda) \cdot (r_{lut} - r_{pxl})^2\right]^{1/2}}{\sum w(\lambda) \cdot r_{pxl}}$$

where r_{lut} and r_{pxl} are the values, per band, for the modelled LUT values and the pixel value it is being compared to respectively, and $w(\lambda)$ is a per-band weighting function defined by the Noise Equivalent Reflectance Difference (see Brando et al. 2009 for details). Upon calculating optical closure for all of the R_{rs} values in the LUT, environmental variables from the R_{rs} with the closest optical closure are assigned to the pixel.

3. Python Model

The water quality model described above, and the process for inverting the model to estimate water quality from imagery, has been coded into a python script. The script must be run using Python 3 but is OS-independent. In addition, the following python libraries must be installed: numpy, osgeo (gdal), ElementTree, matplotlib, and pyproj.

3.1 List of Files

The complete list of script and data files are as follows, found within the /Code/ folder in the files archive associated with this report:

- *main.py* - the main implementation of the script, also where all user inputs go
- *functions.py* - general functions for the script operation
- *waterQualityModel_hyperspec.py* - the water quality model equations, parametrized for hyperspectral imagery
- *bandInfoProcessing.py* - functions for accessing band metadata and processing band data
- *pointSpectrumExtraction.py* - functions for extracting spectral data from imagery at coordinate points. Note: Currently, UTM zone is hard-coded for Quesnel Lake in this file!
- *modelInverstionFunctions.py* - functions for inverting the water quality LUT
- *graphingFunctions.py* - functions for graphing output modelled spectra
- /model_data/ - this folder contains spectral data needed for running the model
    - *absorption_spectra.npy* - absorption spectra for pure water and phytoplankton, in numpy array format
    - *wavelengths_list.txt* - list of wavelengths to be modelled over. By default, this is 395.00 nm to 1004.80 nm, in increments of 0.20 nm, to cover the range of the DESIS sensor.
    - *LUT.npy* - if present, a pre-constructed look-up table of modelled spectra. If not present, it will be created in the script and deposited here.
- /outputs/ - this is an empty folder into which the modelled concentration values for points, and graphs of modelled spectra will be deposited when the model is run.

3.2 User Inputs

In *main.py*, the first block of code includes the user input section.

```
#########################################################
### User Input ###

# Imagery:
imagery_infile = 'imagery/DESIS-HSI-L2A-DT0466548128_002-20200619T174938-V0210-SPECTRAL_IMAGE.tif'
metadata_infile = 'imagery/DESIS-HSI-L2A-DT0466548128_002-20200619T174938-V0210-METADATA.xml'

# Sample point coordinates:
sample_points_infile = 'imagery/sample_points.txt'

# Define concentrations bounds: (start, stop, interval)
bounds_C_nap = (1., 1000., 400.)
bounds_C_chl = (1., 1000., 200.)
bounds_C_cdom = (1., 1000., 200)

# New or Existing LUT?
create_LUT = 'FALSE' # 'TRUE' or 'FALSE'
existing_LUT = "model_data/small_test_LUT.npy" # if 'FALSE', will import existing LUT

#########################################################
```

Here, the user must define:

- **imagery_infile** - the path (relative to working directory, like in the example above, or absolute) to the .tif file for the DESIS image.
- **metadata_infile** - the relative or absolute path to the associated DESIS metadata file
- **sample_points_infile** - the relative or absolute path to the location of sample points in the imagery on which the model will estimate water quality. These must be a space- or tab-delimited list of coordinates (latitude longitude) in WGS84 decimal degrees, and can include any number of coordinates **greater than or equal to 2**. For example:

  ```
  52.489028 -121.451204
  52.572558 -121.540309
  52.514256 -121.602020
  52.562675 -121.615120
  ```

- **bounds_C_nap/chl/cdom** - the upper and lower bounds for the range of concentration values (mg/L) which will be forward modelled for TSS (*nap*), chlorophyll-a, and CDOM respectively. These must be in a tuple (bracketed list), including (upper bound, lower bound, interval), each

in float format. For ease of design, each value must either have a decimal place (ex. **2.5**), or end in a decimal (ex. **2.**)

- **create_LUT** - whether a new LUT will be created using the above bounds (**'TRUE'**), or whether an previously-made LUT will be imported (**'FALSE'**). Since LUT construction is the most time-consuming aspect to this code, importing an existing one will always save time.
- **existing_LUT** - the relative or absolute path to an existing LUT in the .npy file format. Since the format of the LUT must be the same as is expected by the code, it is best to use an LUT which has previously been generated by the code itself. If a new LUT is being constructed (i.e. if **create_LUT = 'TRUE'**), then the content of **existing_LUT** is irrelevant.

3.3 Code Structure

The basic structure of the code follows the three-step process outlined in section 2.2 above: 1) Creation of a look-up table using the water quality RTM, 2) extraction of spectral data from the imagery, and 3) model inversion to find the closest LUT match to each image spectrum; and 4) an additional step to export results and graph modelled spectra.

1) LUT Creation

This section is only run if **create_LUT = 'TRUE'**; otherwise, it is skipped and an existing LUT is imported later.

First, an LUT shell is created using **createLutShell()**, which permutes every combination of water constituent concentrations according to the input bounds (start, stop, interval) for each of the three constituents NAP, CHL, and CDOM; one permutation per row of the LUT. The function also creates empty columns in the LUT into which the modelled band values will be stuffed during modelling.

Next, for each row of the LUT (i.e. each permutation of the water constituent concentrations), **waterQualityModelling()** calculates the expected water-leaving remote sensing reflectance *Rrs* as a function of wavelength, for each wavelength in */model_data/wavelengths_list.txt* . This continuous spectrum is then convolved into band values using **spectrumConvolution()**, which uses the sensor's spectral response function found in the imagery metadata to "simulate" what each band in the sensor would see given that modelled continuous spectrum. These modelled band values are then stuffed into the LUT by **populateLUT()**.

The LUT is then exported as a .npy numpy array and deleted from memory.

2) Imagery Spectrum Import

Sample points are used to extract spectral data from the imagery at coordinate locations, using the function **extractValuesFromList()**, and saved into a text file.

3) Model Inversion

Either the newly created LUT, or an existing LUT is loaded back into memory in **mmap_mode = 'r', which** *significantly* improves the speed of processing, and reduces memory load on the system.

Instead of loading the entire LUT into memory at once, the file is sliced into smaller sections and only the section currently needed is read into memory.

The model inversion runs on each sample point's imagery spectrum, where **findBestLUTFit()** calculates the Root Mean Square Error between the modelled and imagery-observed band values, and finds the LUT row (and thus the water constituent concentrations) in which the modelled spectrum most closely resembles the observed spectrum.

The resulting water constituent concentration values for each sample point are then exported.

4) Graphing

The modelled and observed spectrum are then graphed for each sampling point, first using **getCentralWavelengths()** to extract from metadata the band centres (to be used on the x-axis), and then **graphSamplePoints()** to generate the graphs. The blue line indicates the imagery-observed spectrum and the orange line indicates the closest-matched modelled spectrum.

3.3 Code Improvements

This section lists some changes or improvements which can be made to the code:

- Instead of importing the wavelengths list over which to be modelled, it should be relatively simple to generate the list programmatically using the range() function. However due to problems with non-integer intervals a list was created manually and imported.

```
# Import list of wavelengths to model for:
wavelength_list = np.genfromtxt('model_data/wavelengths_list.txt').tolist() # list of wavelengths to model over
```

- Once field data is available, the sample points at which imagery spectral data is extracted will match the locations of field samples. When this is the case, it will be useful to create and output a scatterplot of modelled water constituent concentrations versus the field-measured ones. In addition, if a field-measured spectrum is also taken, this data can be added to the output spectral graphs which are already included.
- The model currently only inverts over discreet sample points, as defined by coordinates in the text file pointed to by **sample_points_infile**. This is useful for model calibration and testing, since we only need to be able to compare points of known water quality to our model output. Only inverting on these field point locations, instead of on the entire water-covered portion of an image makes the inversion process much *much* faster. However, once we are satisfied with the performance of the model and want to start mapping water quality over the whole lake, we will need to invert for each pixel. This will require an overhaul of the inversion portion of the code, but may be done using some variation of:
    - Import each band as a numpy array using **gdal.BandReadAsArray()**
    - Save each band as a .npy file using **np.save()**

- Import each band as a numpy array in **mmap_mode = 'r'** using **np.load()**
- Loop over each pixel in imported image (skipping non-water pixels based on a land-mask) using **for y, x in np.ndindex(band_array.shape):**
- Extract the band values at each pixel and run the inversion as normal.

This will be computationally intensive, so if time was a consideration it may be useful to only run the inversion on some multiple of pixels, like every 10th pixel in the x and y directions, and interpolate between the inverted pixels. Since water quality changes slowly spatially, this simplification should hold.

4. Imagery

4.1 Multispectral vs Hyperspectral: The Problem of Non-Uniqueness

The concept of non-uniqueness, simply put, is that there is more than one combination of environmental variable values which produce the same R_{rs} spectrum (Sydor et al. 2004).

With the relative lack of spectral information present in each pixel of a multispectral image, more than one combination of reasonable concentrations of chl-a, TSS, and CDOM; and reasonable depths and bottom reflectance factors, can create the same R_{rs} (or close enough to be within imaging error). In fact, as will be demonstrated shortly, there are not only a few identical spectra, there are possibly hundreds, and the different combinations of environmental variables aren't only a bit different, they're drastically different, which is a catastrophic problem for the method when using multispectral imagery, and a solution has as yet not been proposed.

Figure 4 shows an example of some data from a previous project for which field-measured water quality values exist, showing the results of modelling NAP (which is similar to TSS), chl-a, and CDOM for two optically deep sections of South Nation River near Ottawa, specifically for a single pixel closest to the location of each field sample. The black points are the *Rrs* spectrum from the atmospherically corrected WorldView-3 imagery (similar spectral properties to Landsat 8), green is the modelled spectrum with the closest match to the observed (black) points from the LUT, and the continuous dark blue line is a continuous spectrum modelled using direct field measurements of the water constituents. Ignore the light blue dashed line for now. The LUT used here has 132,799 modelled spectra.

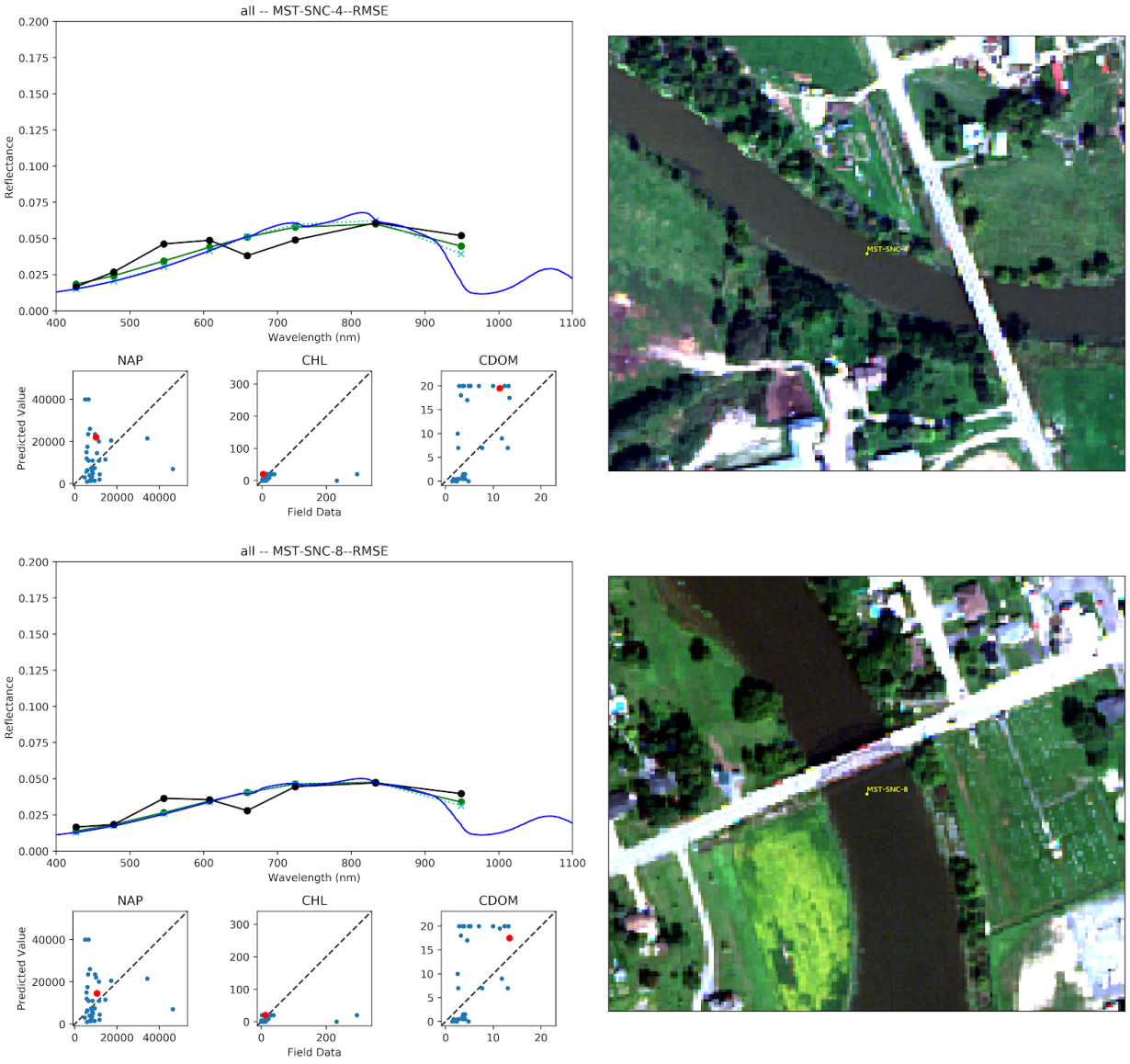

Figure 4: Modelling results for two optically deep sections of South Nation River. The yellow marker on the WorldView-3 imagery shows the location of the field sample. The three scatterplots along the bottom show field measured vs. modelled values for NAP, CHL, and CDOM; with the red dot indicating the results of the currently-shown location. The spectral plots show (Black) the imagery-observed spectrum, (Green) the modelled spectrum with the closest spectral match to the imagery-observed spectrum, (Dark Blue) the continuous spectrum modelled using field-measured concentration values, and (Light Blue) the LUT spectrum with the closest match to field-measured concentration values.

Though the green line and the black line match up reasonably well, indicating that the optical closure procedure worked well to find a close match between observed and modelled spectra, in the validation scatter-plots below the main plots, it is clear that the correct values for the water constituents were not found. To check whether the LUT entry with the *correct* constituent values also looks similar to the black line, instead of matching LUT entries by closest match to spectrum, we can find the LUT entry

with the closest match to the field data, which is the light blue dashed line in the main plot. It is clear that the modelling was done reasonably correctly, since the light blue line also matches well with the observed spectrum. What we are seeing here is the beginnings of the evidence of non-uniqueness.

To directly attempt to measure non-uniqueness, we can run an experiment on the LUT table and the observed R_{rs} spectra where, instead of finding the *single* LUT entry with the closest optical closure, we can find *all* LUT entries within some threshold of optical closure. Figure 5 shows the readout for the SNC-8 field site (bottom site in the two panels above), where the LUT entries within an RMSE of 0.002 (of R_{rs}, unitless) are gathered.

```
matus@matus-work:~/Documents/Contracts/AgCan/Script$ python3 nonunique_testing.py

Target Curve: LUT index =  32991
 [ 0.01316849  0.01766217  0.02586556  0.0340941   0.04055243  0.04642384
  0.04727562  0.03147552]

RMSE Threshold =  0.002

Number of matched curves =  1289
Number after trimming   =  13

ENVIRONMENTAL CONCENTRATION

NAP             CHL             CDOM
6000.0           3.0             9.0
8000.0           6.5             10.5
9000.0           8.0             11.5
9500.0           11.0            13.5
10000.0                  14.0            11.5
10500.0                  16.0            13.0
11000.0                  17.5            12.5
11500.0                  18.0            14.0
12000.0                  18.0            15.5
12500.0                  18.0            15.5
13000.0                  18.5            14.0
13500.0                  19.0            16.0
14500.0                  17.0            18.0
matus@matus-work:~/Documents/Contracts/AgCan/Script$
```

Figure 5: Readout for the non-uniqueness experiment, showing 1289 LUT spectra within 0.002 RMSE of the target spectrum, out of a total of 132,799 spectra.

First, notice that there are 1289 LUT entries which fall within this RMSE threshold, out of a total of 132,799 LUT spectra. Displayed and plotted in green in Figure 6 are every 100th matched curve for a total of 13 (in comparison to the observed *Rrs* in black), since plotting all 1289 would not be practical. Second, notice that the water constituent values (in Figure 5), whose corresponding modelled *Rrs* spectra were all nearly identical to each other, have a massive range, essentially covering the entire range of values which were used to generate the LUT.

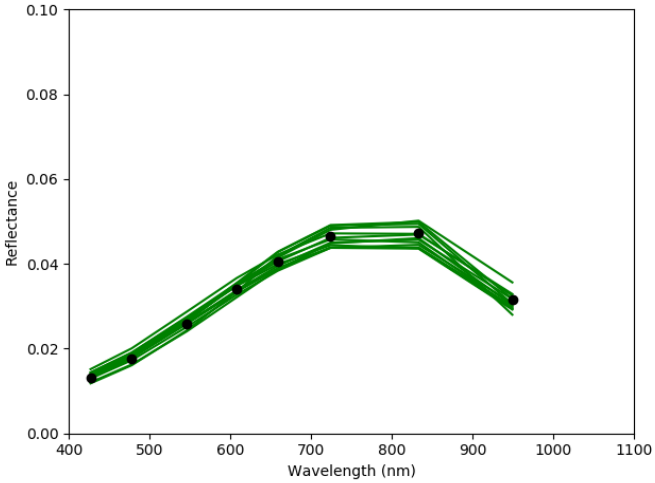

Figure 6: Thirteen of the 1289 similar spectra from the non-uniqueness experiment.

So not only are there an overwhelming number of non-unique options for spectra which look similar to the spectra observed in the imagery in this example, their range is such that the predictions would not even be useful to get a basic idea of the water quality in the area. Thus, to get accurate water quality readings, we need to use hyperspectral imagery, which will give more spectral information per pixel, and hopefully be able to better resolve differences in water quality.

4.2 DESIS Hyperspectral Imagery

The DLR Earth Sensing Imaging Spectrometer (DESIS), mounted on the International Space Station (ISS), provides 235-band hyperspectral imagery, between 400 and 1000 nm, at a spatial resolution of 30 m (Krutz et al. 2019). Being mounted on the ISS provides for cheaper installation and the possibility of repair, however due to the station's orbit plan image acquisitions are limited to below about 51°N latitude. With a pointing capability of 15° off-nadir, imagery may be collected at slightly higher latitudes, though Quesnel Lake's latitude of 52.5°N puts it near the northern edge of what is possible to image with DESIS.

For modelling, 60-channel Level2A (L2A) imagery was used. This imagery is modified from its original 235-band form by 4 band binning, which provides a contiguous spectral range from 400-1000nm with spectral sampling resolution 10.2 nm and Full Width Half Maximum of ~7.0 nm. The binning allows for increased signal-to-noise (S/N) and as no spectral features with FWHM of 10 nm or less was expected in the data for modelling, and the radiometry of low magnitude, this seemed like the best choice.

One of the earlier images acquired by this DESIS for this project is a 60-band image from 19 June 2020 showing the western half of Quesnel Lake, Hazeltine Creek and the Mount Polley Mine. The image is an Atmospheric Compensated Product (L2A), which uses an atmospheric correction algorithm based on ATCOR to retrieve surface reflectance (Alonso et al. 2019). DESIS data acquisition remains ongoing through 2022. At the time of publication DESIS imagery acquired over

this location could be accessed after submitting a request via the DLR Earth Observation Center EOWeb GeoPortal (EOWeb.DLR.de/EGP/).

4.3 Landsat Multispectral Imagery

Though, as described above, multispectral imagery suffers from the issue of non-unique solutions to model inversion, Landsat 8 multispectral imagery has a key advantage over DESIS hyperspectral imagery: There exists a freely available imagery archive of the entire planet, with imagery captured every 16 days (though useful imagery is less frequent due to clouds), with imagery available from before the Mount Polley spill. This comprehensive archive of imagery may allow us to retroactively measure water quality before, during, and for a long time after the spill, should the non-uniqueness issue be solved.

Two Landsat 8 scenes were acquired at the time of the August 4th tailings pond breach, one just before (LC80470232014210LGN01 acquired July 29th) and one soon after (LC80480232014217LGN01 acquired August 5th). At the time of publication these were freely available from various archives (such as the USGS at EarthExplorer.USGS.gov or via the Google Earth Engine)

5. Field Methods

The purpose of fieldwork for this project is to gather field measurements of water quality (concentrations of TSS, Chlorophyll-a, and CDOM), as well as water-leaving reflectance, for the purposes of calibrating and validating the model. Ideally, measurements would be taken during satellite overpass to get concurrent imagery and field data. Water quality may be measured using an optical sonde suspended in the water column, and water-leaving reflectance may be measured using a two-channel spectrometer set up within a Skylight-blocked system.

5.1 Water Quality Sonde

Prior to renting a water quality sonde, a review was performed on sondes available on the market, with the intention of purchasing a sonde rather than renting. It was later determined that renting would be the better option for the first field work season, to get an idea of how the sondes worked before committing to the purchase of the equipment, which typically costs upwards of $20,000. Though no sonde was purchased, the information below has been included in this report to aid in purchasing decisions for future researchers in this field should that be helpful.

Three specific water constituents need to be measured, to correspond with the three modelled constituents: Coloured Dissolved Organic Matter (CDOM), Turbidity, and Chlorophyll-a. Since no single for-purpose sonde exists to measure all three, a customized multiparameter sonde needed to be built incorporating these sensors. In addition to these three sensors, it would be beneficial to have the possibility to later add additional sensors and capabilities to the sonde for other potential water quality measurements. Specifically, these include a conductivity sensor to determine salinity, and a depth sensor to allow for depth-profiling of quality down through the water column.

Two manufacturers are capable of constructing these customized multiparameter sondes: *Yellow Springs Instruments* (YSI), and *Eureka*, for which Hoskin Scientific Ltd. and Geoscientific Inc. are the respective distributors in Canada. YSI offers the EXO line of probes, and Eureka offers the Manta line of probes. Table 1 compares the EXO1 and the Manta+3.5, the models identified by each distributor to be the most appropriate for our needs as outlined above. Though the Manta probe is slightly more expensive than the base-model EXO1, it has many more capabilities which need to be purchased as extras for the EXO1 probe (extras shown in red), leading to a significantly higher purchase price. For this reason, it was determined that the Manta probe provides more value for the price.

Table 1: Instrument comparison of the two water quality sondes deemed most appropriate for this project, the YSI EXO1, and the Eureka Manta.

	EXO1	**Manta**
Total Price **(base configuration)** **(upgraded configuration)**	**$20,570** **$30,424**	**$24,485** --
Sensor attachments	Conductivity/Temperature *(0 to 100: ±0.5% of reading or 0.001 mS/cm, w.i.g.; 100 to 200: ±1% of reading)* fDOM/CDOM *(Linearity: R2 >0.999 for serial dilution of 300 ppb QS solution Detection Limit: 0.07 ppb QSE)* CHL-a *(0 to 100 RFU; 0 to 100 µg/L PC)* Turbidity *(0 to 999 FNU: 0.3 FNU or ±2% of reading, whichever is greater; 1000-4000 FNU: ±5% of reading)* **Depth to 100 m[1] ($545)**	Conductivity/Temperature *(temp -5°C – 50°C ±0.1°C; cond 0 – 100 mS/cm ±0.5% reading + 1 count)* fDOM/CDOM *(0-1250 ppb)* CHL-a *(.03 - 50µg/L +/- 3%)* Turbidity *(0 – 3000 NTU 0-100 ±< 1% of reading, 100-400 < 3% of reading, over 400 < 5% of reading)* **Depth to 25 m**
Accessories	Carrying case **Calibration cup[2] ($290)** **Turbidity standard solution[3] ($1830)** **Anti-fouling wiper[4] ($1,904)**	Carrying case Calibration cup Turbidity standard solution Anti-fouling wiper
Interface	**Tablet interface ($4,256)** **10 m field cable[5] ($1,029)**	Bluetooth transmitter, used with phone app 20 m field cable

[1] Depth sensor may be used for depth-profiling through the water column
[2] To hold the sensor while calibrating
[3] A solution with a precisely known turbidity, for calibrating the turbidity sensor
[4] A rotating wiper blade to scrub sediments off the sensor heads, allowing for continuous monitoring without the need to manually clean the sensor heads frequently.
[5] Cable for attaching the instrument to a read-out device or Bluetooth transmitter, to allow for initializing the instrument in the field (rather than in the lab prior to heading out), and for real-time monitoring of readings to ensure good quality data is being gathered.

As the preparation for field work during the first summer or COVID progressed, it was determined that a rental unit was more appropriate than purchasing a sonde, so an EXO1 sonde from Hoskin Scientific was rented, as the Manta probes didn't offer rentals. The rented probe was effectively identical to the sonde under consideration for purchase, allowing us to evaluate its effectiveness before purchase (Figure 7).

QTY	ITEM	DESCRIPTION	BILLABLE DAYS	SERIAL NO.	UNIT PRICE	EXTENDED PRICE
1	R-E528-599501-02-01	Exo1 Sonde 100M Depth	08/20/20 - 09/11/20	12F101882	1,395.00	1,395.00
1	R-E528-599101-01-05	Exo Turbidity Sensor	08/20/20 - 09/11/20	18K100344	0.00	
1	R-E528-599104-01-01	Exo Fdom Sensor	08/20/20 - 09/11/20	12F100203	0.00	
1	R-E528-599102-01-02	Exo Total Algae-PC Sensor	08/20/20 - 09/11/20	13D100700	0.00	
1	R-E528-599960-09	Exo Handheld Display 2.0	08/20/20 - 09/11/20	18C102275	0.00	
1	R-E528-599040-66-07	EXO Field Cable	08/20/20 - 09/11/20	200221-66	0.00	
1	R-E528-599810-07	Exo Output Adapter-USB	08/20/20 - 09/11/20	12390942	0.00	

RENTAL PERIOD: 08/20/20 TO 09/11/20	RENTALS	1,395.00
	MISCELLANEOUS	0.00
	FREIGHT	0.00
	BC PST	97.65
	TPS/GST	69.75
INVOICE Hoskin Scientific Ltd (VAN) G.S.T.#743312498	**Total CAD:**	**1,562.40**

Figure 7: Receipt from the rented water quality sonde used for fieldwork, showing the configuration of the modular sonde attachments.

When rented, the water quality sonde comes pre-calibrated from the rental company, and use simply involves charging the battery, suspending the sonde in the water, and starting recording on the handheld unit (after setting a sampling interval). Once survey is complete, the water constituent concentrations may be downloaded from the handheld-unit; readings are time-coded.

5.2 Spectrometer

An Ocean Insight Jaz spectrometer was used for measuring water-leaving reflectance, having a spectral range of 200 - 1100 nm at a resolution of 0.3 to 10.0 nm. The spectrometer was set up with two channels to allow for an upwelling (water-viewing) and downwelling (sky-viewing) component, to easily calculate reflectance values. Critically, the spectrometer is operated using a "skylight blocked approach" (SBA), which allows the water-viewing component to measure only water-leaving reflectance (i.e. light which has passed through the water column), and omit water-surface reflectance, in which light has not interacted with the water column, and thus does not contain information about water constituents (Lee et al. 2013); the particular setup will be discussed in section 5.3. For the sky-

viewing spectrometer component, a cosine corrector must be added to the spectrometer head, which allows for the gathering of light from a 180° field of view.

Operating the spectrometer:

The night before the field survey, make sure to hook the spectrometer up to charge, and that an SD card is inserted. Only SD cards of 2 GB or less work in the spectrometer, and these are hard to find these days, so plan well ahead of the survey date to source one online, since you won't be able to find them at electronics shops.

When connecting the cables to the spectrometer, ensure that the sky-viewing cable is connected to Module 2, which is the one closest to the buttons and screen. Connect the water-viewing cable to Module 3, which is the one on the end farthest from the buttons and screen. It is also useful to use stickers to label both the spectrometer body and the ends of the fibre optic cables as "sky" and "water" to not get them confused.

When surveying:

1. Turn on the spectrometer using the power button
2. When the system turns on, you are asked to select Module 2 or Module 3. Instead, use the red X button to go back on level.
3. Select *Module 2 > System Tools > Time and Date > Acquisition Parameters* and set Boxcar to 5 and Averaging to 11.
4. With the sky-viewing spectrometer head in it's tube, and unobstructed, select *Integration Time > Auto* and record the value. Go back to *Integration Time*, and manually set a time which is 2/3rds of the auto-generated time.
5. Navigate to Scope mode, look at the graph on the display, and ensure that no part of the graph reaches above the screen (i.e. is saturated).
6. Repeat Steps 3-5 for Module 3, ensuring that the SBA tube is suspended in the water with the spectrometer head correctly installed.
7. Use the red X button to navigate back to the main menu. Select *System Tools > Auto-Save > Change Period*. Select a period between 2 and 5 seconds.
8. Cover the ends of both spectrometer heads with your hands or other completely opaque items. Navigate to *System > Auto-Save > Enable*, wait 10 seconds, then *Disable*. This measures light entering the spectrometer from elsewhere in the system, in case there is a loose connection somewhere.
9. When ready for surveying, navigate to *System > Auto-Save > Enable* again to turn on logging. Since the buttons are fiddly and sometimes don't press properly, ensure that the screen now says *Disable*; this indicates that the device is logging.
10. When surveying is complete, select *Disable*.
11. Remove the SD card and copy the data to a computer. Clear the SD card in preparation for the next survey day.

If the spectrometer body overheats, it may power off. Ensure that the spectrometer body is shaded from direct sunlight, and on particularly hot days, it may be necessary to fill Ziplock bags full of cold

water from overside, and place them next to the spectrometer to cool it off. Periodically replace the water as it heats up. Also, periodically ensure that the spectrometer still displays Disable, showing it's still logging, since it may stop logging for any number of reasons and will need to be turned back on. If the spectrometer itself powers off, the entire set-up process will need to be repeated, which is quite difficult to do when under way, so it is vital to prevent the spectrometer from overheating.

5.3 Setup for Summer 2020

This section describes the setup used during the short Summer 2020 fieldwork season.

Spectrometer and SBA

The water-facing spectrometer head is housed in an SBA unit comprised of an angled PVC pipe (Figure 8). The spectrometer head is situated within the pipe such that the field of view of the spectrometer does not intersect with the pipe.

Figure 8: the water-facing spectrometer head, housed in an angled grey PVC pipe, used to shade the water being observed, to prevent water reflection. Notice the black line on the pipe near the water, indicating the location of the end of the spectrometer, which must remain above water during measurement. Photograph by M. Hodul. NRCan photo 2022-309.

The small black line around the tube just above the water surface indicates the position of the spectrometer head, and the end of the skylight blocking tube is in the water. While surveying, it is critical that the end of the tube remain in the water to prevent skylight from polluting the reading, and that the spectrometer head (thus the black line) remain above the water to prevent readings from below the water surface (as these would not take into account the effect of surface refraction and would thus be erroneous readings). It is thus important to prevent the vessel onto which the system is mounted

from tipping too much. For this, and various other reasons, it is advisable to only measure on days in which the weather is relatively calm.

The sky-viewing spectrometer component must be affixed at the top of a post such that it is the highest thing on the vessel (including the surveyor's head), so that it has an unobstructed view of the sky.

Sonde Housing

The water quality sonde is housed within a large PVC tube on a hinged assembly so it may be taken in and out of the water when wading through shallow sections, and when motoring fast, so as not to damage the sonde (Figure 9). The bottom of the tube is perforated, so water can run freely through the tube and past the sonde's sensor heads when in use. A paddle was used to keep the housing suspended up, as seen in the image.

Figure 9: Housing for water quality sonde, currently being held up by paddle for travelling quickly between observation sites. The hinged assembly allows it to lower into the water during measurement. Photograph by M. Hodul. NRCan photo 2022-310.

Complete System

Figure 10 shows the complete system, showing the sky-viewing component on its pole (A), and the water-viewing component in its SBA housing (B). Notice also that (B) is positioned far away from the hull of the vessel, in order to prevent shading of the water column by the vessel itself. In ideal survey conditions, the boat would be oriented such that (B) is *between* the sun and the boat, so that the shadow of the hull is cast away from where the spectrometer is observing, rather than casting a shadow onto that area. In reality, and especially in rivers where boat orientation is not an arbitrary luxury, this may be difficult or impossible to achieve.

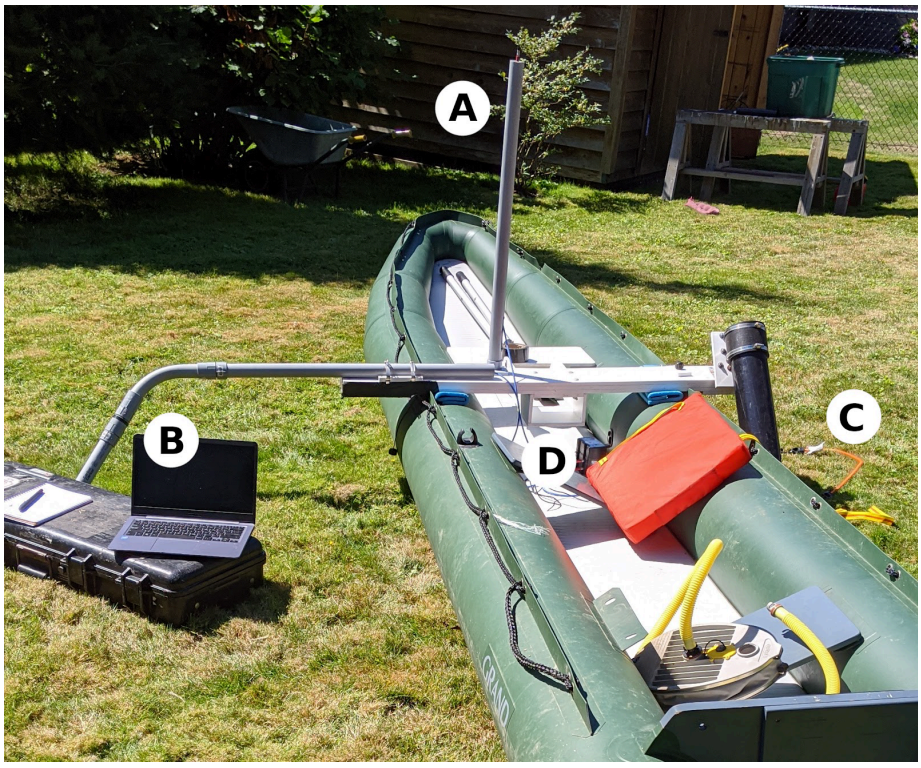

Figure 10: Overview of the complete setup, showing (A) the sky-viewing spectrometer head, (B) the water-viewing spectrometer head, (C) the water quality sonde and housing, and (D) the instrument zone where logging units for spectrometer and sonde sit. Photograph by M. Hodul. NRCan photo 2022-311.

The water quality sonde assembly is on the opposite side of the boat (C). Inside the boat, there is a space for the spectrometer and the handheld monitor for the water quality sonde to safely sit (D). A GPS unit was also used to record position information.

The rest of the system consists of the boat itself, a soft-bottomed inflatable dinghy, and a 6 HP internal-tank outboard motor (Figure 11). This boat was rather narrow, which made it very tippy and difficult to walk around in; a wider, shorter boat would be better next time. Ideally, the boat would have an electric trolling motor in addition to the gas motor, for the quiet, slow movement needed for surveying. Movement of the boat should be limited to the slowest possible speed given the motor used, to reduce wake around the sampling heads.

Figure 11: The boat used, complete with motor and a day's worth of provisions. Photograph by M. Hodul. NRCan photo 2022-312.

Another option for a fieldwork setup would be a separate, small floating platform holding all of the instruments, towed behind the boat. Such a system was used to good effect for some previous surveying in Nunavut (Figure 12).

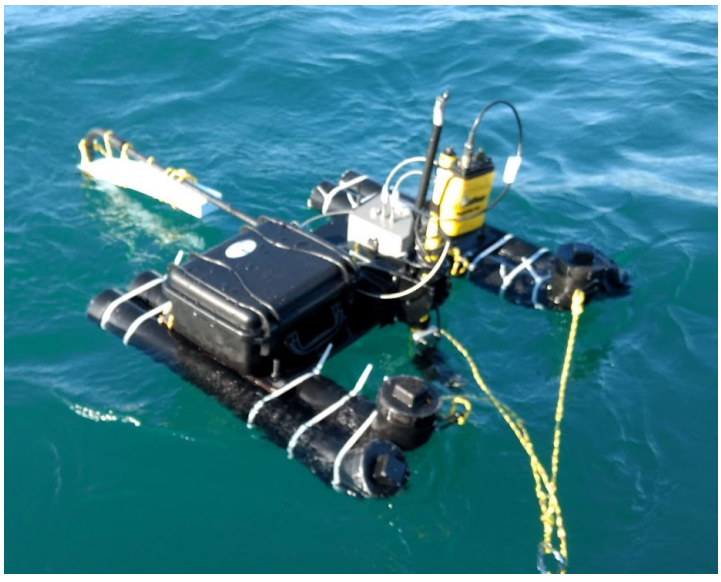

Figure 12: An alternate approach to the SBA system is to have everything on a separate floating platform towed behind the survey vessel, as seen here, which is a system used for similar work in Nunavut. Photograph by M. Hodul. NRCan photo 2022-313.

6. Field Data from Summer 2020

The purpose of fieldwork this summer was to begin to develop a large dataset connecting hyperspectral water-leaving reflectance values to coincident water quality measurements. These data will then be used to investigate non-uniqueness in semi-analytical water quality mapping using satellite imagery, to investigate which sensors are more or less prone to non-uniqueness, and to help develop methods for mitigating the effects of non-uniqueness through environmental context data.

Due to the travel restrictions and other effects of COVID-19 restrictions and lockdowns in both BC and at the University of Ottawa, the field season was mostly cut off from late April to around mid-July. Further, the University field safety department's new application procedure and checks meant that my work was unable to get off the ground until the end of August. For these reasons, a limited number of study areas were measured at (Table 2).

Table 2: A summary of measurements gathered for each study area:

Location	Date	Spectroscopy Points	Water Quality Points	Overpass
Alouette Lake	2020-09-02	763	3742	S2 (cloudy)
Pitt Lake	2020-09-04	549	3161	None
Pitt River	2020-09-04			None
Sumas River	2020-09-08			L8
Chilliwack River	2020-09-08	664	4869	L8
Fraser River	2020-09-08			L8
Sumas River	2020-09-09			S2
Chilliwack River	2020-09-09	814	6247	S2
Fraser River	2020-09-09			S2

All field location water bodies (Figure 13) were accessible directly via a boat ramp, or by travelling from a boat ramp to the location. Parking was available at all locations. Pitt Lake and Pitt River were accessible from the boat launch at Grant Narrows Regional Park (49.3493, -122.6153). The boat launch is right on the border between the lake and the river, so Pitt Lake can be accessed by going north from here, and Pitt River by going south. Alouette Lake can be accessed through the Alouette Lake Boat Launch (49.2937, -122.4885) in Golden Ears Park. Sumas River, Chilliwack River, and the section of Fraser River sampled are all accessible from the Barrowtown Boat Launch (49.1154, -122.1107). When putting in here, you are in the Sumas River. Travelling north you can reach the Fraser, and forking off southeast at 49.1264, -122.0983 gets you to the Chilliwack River.

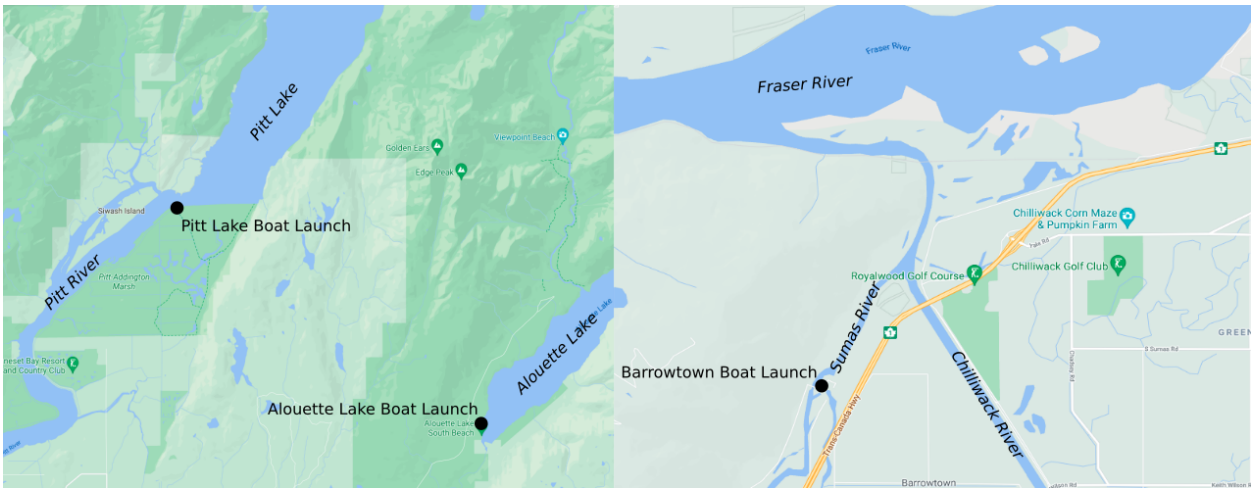

Figure 13: Details of entry points to field sites, showing boat launches at Pitt Lake (49.3493, -122.6153), Alouette Lake (49.2937, -122.4885), and Barrowtown (49.1154, -122.1107).

Field data was somewhat limited due to an equipment malfunction in the GPS unit, which was only discovered on the last day; thus GPS positions for the field samples are only available for 9 September. Though this limits the data's usefulness when comparing it to satellite imagery, clear imagery was only available for the 8th and 9th, so the GPS malfunction only reduces the usefulness of one day's survey. Matchups between water-leaving reflectance from the spectrometer and water quality from the sonde are the more important data, as they will be used to calibrate the models, and these were gathered for all days.

Field data has been compiled into the data archive associated with this report, in the /Field Data/ folder. Here, GPS, Spectrometer, and Water Quality data have been separated into respective folders. Spectrometer data has been further separated into folders based on survey day, since there are individual files for each sampling of the spectrometer.

Each spectrometer file contains date and time information for the sample, as well as spectral information in two columns. The first column shows the wavelength of the band, and the second column shows the radiance measures. The files have been renamed to follow a useful naming convention: The filename begins with an 's' or 'w' indicating whether it is for the sky-viewing or water-viewing component of the spectrometer, followed by the complete date and time as YYYY-MM-DD-HH:MM:SS.jaz

7. Further Research

The purpose of this document is to provide a complete description of the project methods and data thus far and to allow for a researcher to continue the project from where it was left off. To this end, the intended next steps of the project, as well as possible longer-term research directions, will be outlined here.

7.1 Project Next Steps

The immediate next step for the project would be the gathering of field data at Quesnel Lake, including water quality parameters and spectral data, as described in Section 5. Ideally, this data would be measured concurrently with the capture of DESIS imagery. This data could then be used to calibrate the water quality model to the environmental conditions in Quesnel Lake, as well as for model validation. It may also be possible to gather historic water quality data, though the likelihood of such data coinciding with a DESIS overpass are very low, and there likely will not be concurrent field spectral data.

With useful field data and concurrent DESIS imagery leading to a well-calibrated water quality model, the code can then be modified to invert the model over all water pixels instead of only over sample points.

7.2 Further Research

Several areas of further research may stem from a successful application of the water quality modelling with DESIS imagery.

Non-Uniqueness in water quality inversion, I: Quantifying the problem in existing sensors, and proposing a hypothetical "ideal" sensor

Research Questions:

- Does the non-uniqueness problem still exist to some degree when using continuous or hyperspectral water-leaving reflectance data?
- How can we quantify non-uniqueness and to what extent does it exist in existing sensors?
- Can we design a hypothetical spectral response function for a hyperspectral sensor which would minimize non-uniqueness?

Details:

Water-surface spectrometer data gives an effectively continuous spectral signature of the water. Since the spectrum is continuous, there should be little or no non-uniqueness when using it in a physics-based water quality inversion. As we progressively reduce the spectral resolution of the dataset, at what point does non-uniqueness begin to be a problem? We can also model existing sensor spectral responses (with "perfect" atmospheric correction), and see which ones have better or worse non-uniqueness issues. Then we can propose a hypothetical sensor which will minimize non-uniqueness

while still being reasonable to build and deploy (reasonable spectral response, multispectral). We will need to develop some quantifiable measure of non-uniqueness.

Non-Uniqueness in water quality inversion, II: Mitigating the problem using environmental context data

Research Question:

- Can information external to the imagery (environmental context data) be used to mitigate non-uniqueness?

Details:

Another way to minimize non-uniqueness may be to introduce data external to the imagery (environmental context data ECD), either statistically through machine learning, or physically, directly in the physics model. Initially, the selection of which ECD to use will likely be determined statistically. ECD such as local surficial geology/sediments, historical precipitation data, or shoreline slope angles can be added to a statistical water quality predictor such as Random Forest or MARS algorithms, and feature importance can be measured using either an impurity index or a permutation importance method. If a particular ECD feature is deemed to be extremely important to water quality prediction, it may be interesting to try to determine the physical causal reason why this is so, and add it to the physical water quality model.

7.3 Other Areas of Further Research:

- Constraining the model based on the assumption that water constituents do not change drastically over small distances, thus a large change pixel-to-pixel likely represents error.
- Determining more defined spectral properties of TSS, and how knowledge about surficial geology in the area may help predict spectral properties for a particular study site.
- Tightly constraining the model based on known or expected water constituent concentrations to reduce degrees of freedom. For instance, if chl-a concentration can be simply derived from observing absorption at absorption spectra before modelling and using at least a reasonable estimate range to constrain modelling.

8. References

Alonso, K., Bachmann, M., Burch, K., Carmona, E., Cerra, D., de Los Reyes, R., Dietrich, D., Heiden, U., Hölderlin, A., Ickes, J., Knodt, U., Krutz, D., Lester, H., Müller, R., Pagnutti, M., Reinartz, P., Richter, R., Ryan, R., Sebastian, I., & Tegler, M. (2019) Data Products, Quality and Validation of the DLR Earth Sensing Imaging Spectrometer (DESIS). Sensors (Basel, Switzerland), 19(20), 4471.

Brando, V.E., Antsee, J.M., Wettle, M., Dekker, A.G., Phinn, S.R., and Roelfsema, C. (2009) A physics based retrieval and quality assessment of bathymetry from suboptimal hyperspectral data. Remote Sensing of Environment, 113, 755-770.

Byrne P., Hudson-Edwards, K.A., Bird, G., Macklin, M.G., Brewer, P.A., Williams, R.D., and Jamieson, H.E. (2018) Water quality impacts and river system recovery following the 2014 Mount Polley mine tailings dam spill, British Columbia, Canada. Applied Geochemistry, 91, 64-74.

Dekker, A.G., Phinn, S.R., Antsee, J., Bisset, P., Brando, V.E., Casey, B., Fearns, P., Hedley, J., Klonowski, W., Lee, Z.P., Lynch, M., Lyons, M., Mobley, C., and Roelfsema, C. (2011) Intercomparison of shallow water bathymetry, hydro-optics, and benthos mapping techniques in Australian and Caribbean coastal environments. Limnology and Oceanography: Methods, 9, 396-425.

Giardino, C., Bresciani, M., Braga, F., Cazzaniga, I., De Keukelaere, L., Knaeps, E., and Brando, V.E. (2017) Bio-optical modeling of total suspended solids. Bio-Optical Modeling and Remote Sensing of Inland Waters, pp.129-156

Hamilton, A. K., Laval, B. E., Petticrew, E. L., Albers, S. J., Allchin, M., & Baldwin, S. A., et al. (2020) Seasonal turbidity linked to physical dynamics in a deep lake following the catastrophic 2014 Mount Polley mine tailings spill. Water Resources Research, 56(8),

Hatam, I., Petticrew, E.L., French, T.D., Owens, P.N., Laval, B., and Baldwin, S.A. (2019) The bacterial community of Quesnel Lake sediments impacted by a catastrophic mine tailings spill differ in composition from those at undisturbed locations – two years post-spill. Sci Rep, 9, 2705.

Krutz, D., Müller, R., Knodt, U., Günther, B., Walter, I., Sebastian, I., Säuberlich, T., Reulke, R., Carmona, E., Eckardt, A., Venus, H., Fischer, C., Zender, B., Arloth, S., Lieder, M., Neidhardt, M., Grote, U., Schrandt, F., Gelmi, S., & Wojtkowiak, A. (2019). The Instrument Design of the DLR Earth Sensing Imaging Spectrometer (DESIS). Sensors (Basel, Switzerland), 19(7), 1622.

Kutser, T., Koponen, S., Kallio, K.Y., Fincke, T., and Paavel, B. (2017) Bio-optical modeling of colored dissolved organic matter. Bio-Optical Modeling and Remote Sensing of Inland Waters, pp.101-128

Lee, Z.P., Carder, K.L., Mobley, C.D., Steward, R.G., and Patch, J.S. (1998) Hyperspectral remote sensing for shallow waters, 1: A semianalytical approach. Applied Optics, 37(27), 6329-6338.

Lee, Z.P., Pahlevan, N., Ahn, Y.H., Greb, S., and O'Donnell, D. (2013) Robust approach to directly measuring water-leaving radiance in the field. Applied Optics, 52(8), 1693-1701.

Matthews, M.W. (2017) Bio-optical modeling of phytoplankton chlorophyll-a. Bio-Optical Modeling and Remote Sensing of Inland Waters, pp.157-188

Ogashawara, I., Mishra, D.R., Gitelson, A.A. (2017) Remote sensing of inland waters: Background and current state-of-the-art. Bio-Optical Modeling and Remote Sensing of Inland Waters, pp.1-24

Ritchie, J.C., Zimba, P.V., and Everitt, H. (2003) Remote sensing techniques to assess water quality. Photogrammetric Engineering & Remote Sensing, 69(6), 695-704.

Sydor, M., Gould, R.W., Arnone, R.A., Haltrin, V.I., and Goode, W. (2004) Uniqueness in remote sensing of the inherent optical properties of water. Applied Optics, 43(10), 2156-2162.